Chapter 3. Numerical Simulation

This chapter presents different models developed to investigate the potential of an active-passive distributed absorber. A variational method has been used to model different elements such as a beam, springs, actuators and absorbers. No method gives an exact solution for this type of system except for very particular conditions (e.g. simply supported beam). Another approximate method could have been used; namely the finite element method. With this method, the geometry is theoretically not constrained to the beam. It has also some drawbacks. The boundary conditions are difficult to take into account since they act on very few elements of the system. The number of elements used is also a problem especially for high frequency accuracy. The size of the matrices involved increases each time a new element is added which will penalize computation. In this specific research, aimed at investigating the potential of an active distributed absorber, the variational methods seemed appropriate. Optimization was one of the issues and computation time was critical. The variational method is a powerful tool that has met the modeling and optimization challenge in past work. This chapter presents each of the constitutive parts of a global model including a beam, piezoelectric layers (the disturbance), point absorbers, constrained layer damping and a distributed absorber.

3.1 The beam

3.1.1 Theoretical model

The central component of the model described in this chapter is a simple beam. Any boundary condition is modeled using springs of complex stiffness. The material of the beam itself has a complex Young's Modulus in an attempt to model structural damping.

On top of this beam, different type of added layers can be positioned. These layers are part of the distributed devices listed below:

- Mass layer
- Piezoelectric layer
- Constrained layer damping (2 layers)
- Distributed absorber (2 layers)

Figure 3.1 presents the global model of the beam with the different notation associated with it. For the detail of each variable, the reader is invited to consult the list of symbols (page xv). The reference point is the center of the beam. The horizontal direction is called 1, and the vertical direction 3. The position x of any device on the beam refers to the position of the center of the device.

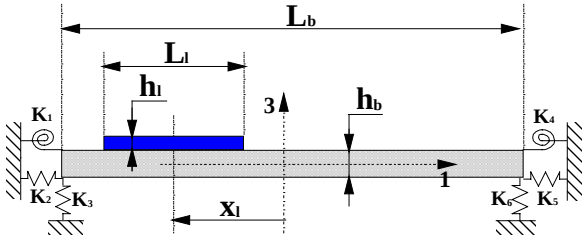

Figure 3.1: Modeled system

The thickness h_l is assumed to be small compared to the thickness of the beam h_b. Since the actuation is asymmetric (in respect to the 1 direction), the axial and transversal motion of the beam is taken into account. Figure 3.2 describes the motion of a slice of the beam and more specifically the motion of a point of the beam. Two different configurations of the beam are considered. The first one is the beam in resting position and is taken as reference. The second configuration is the beam constrained by the disturbance. The width of the beam is assumed to stay constant. A slice positioned at abscise x and of width dx has a horizontal motion $u_b(x)$ and a transversal motion $w_b(x)$.

The rocking of the slice is the first derivative of $w_b(x)$ in respect to x. The vector describing the global motion of the point p is (U_b,W_b).

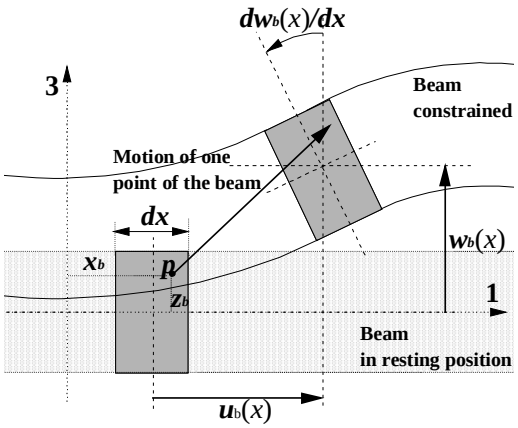

Figure 3.2: Displacement field of the beam

This type of displacement field agrees with the assumption made for a Bernoulli-Euler type beam. These assumptions are that $L_b/h_b>10$ and the amplitude of motion is small. In this type of model, the shear is neglected. The global displacement of the point p is expressed in mathematical terms by equation (3.1). It is expressed in term of the two functions u_b and w_b which vary in time (τ) and space (x). For the many equations that will follow, the reader is invited to refer to the list of symbols page xv.

$$\begin{cases} U_b(x,z_b,\tau) = u_b(x,\tau) - z_b \dfrac{\partial w_b(x,\tau)}{\partial x} \\ W_b(x,z_b,\tau) = w_b(x,\tau) \end{cases} \tag{3.1}$$

Using (3.1) and the IEEE compact notation [10], the strains for the beam are:

$$\begin{cases} S_1^b(x,\tau) = \dfrac{\partial U_b(x,z_b,\tau)}{\partial x} = \dfrac{\partial u_b(x,\tau)}{\partial x} - z_b \dfrac{\partial^2 w_b(x,\tau)}{\partial x^2} \\ S_2^b = S_3^b = S_4^b = S_5^b = S_6^b = 0 \end{cases} \tag{3.2}$$

Knowing the deformation tensor [c^b] for the beam material, the stresses can be easily deducted and are presented in equation (3.3). The Poisson ratio is neglected in this case.

$$\begin{cases} T_1^b = c_{11}^b S_1^b \\ T_2^b = T_3^b = T_4^b = T_5^b = T_6^b = 0 \end{cases} \tag{3.3}$$

The model is derived for a harmonic motion using the convention of equation (3.4).

$$f(x,z,\tau) = f(x,z)e^{-j\omega\tau} \tag{3.4}$$

Using the equations (3.1) to (3.4), the kinetic and potential energies can be derived.

$$\begin{cases} E_k^b = \dfrac{\rho_b}{2}\displaystyle\int_V \left|\dot{U}_b^2 + \dot{W}_b^2\right| dv = -\omega^2 \dfrac{\rho_b}{2} \int_{-\frac{L_b}{2}}^{\frac{L_b}{2}} \int_{-\frac{h_b}{2}}^{\frac{h_b}{2}} \left[\left(u_b(x,\tau) - z_b \dfrac{\partial w_b(x,\tau)}{\partial x} \right)^2 + \left(w_b(x,\tau)\right)^2 \right] dz_b dx \\ E_p^b = \dfrac{1}{2}\displaystyle\int_V S_1^b T_1^b dv = \dfrac{c_{11}^b b}{2} \int_{-\frac{L_b}{2}}^{\frac{L_b}{2}} \int_{-\frac{h_b}{2}}^{\frac{h_b}{2}} \left(\dfrac{\partial u_b(x,\tau)}{\partial x} - z_b \dfrac{\partial^2 w_b(x,\tau)}{\partial x^2} \right)^2 dz_b dx \end{cases} \tag{3.5}$$

Let us denote the trial functions f_n. The unknown functions are expressed in terms of the trial functions.

$$\begin{cases} u_b(x) = \displaystyle\sum_{p=1}^{P} A_p f_p(x) \\ w_b(x) = \displaystyle\sum_{q=1}^{Q} B_q f_q(x) \end{cases} \tag{3.6}$$

From equations (3.5) and (3.6) the kinetic and potential energy can be expressed in term of finite number of coeficients, A_n, B_n.

$$E = -\omega^2 \frac{\rho_b}{2} h_b \sum_{p_1=1}^{P} \sum_{p_2=1}^{P} \left[A_{p_1} A_{p_2} \int_{-\frac{L_b}{2}}^{\frac{L_b}{2}} f_{p_1}(x) f_{p_2}(x) dx \right]$$
$$- \omega^2 \frac{\rho_b}{2} \frac{h_b^3}{12} \sum_{q_1=1}^{Q} \sum_{q_2=1}^{Q} \left[B_{q_1} B_{q_2} \int_{-\frac{L_b}{2}}^{\frac{L_b}{2}} \frac{\partial f_{p_1}(x)}{\partial x} \frac{\partial f_{p_2}(x)}{\partial x} dx \right]$$
$$- \omega^2 \frac{\rho_b}{2} h_b \sum_{q_1=1}^{Q} \sum_{q_2=1}^{Q} \left[B_{q_1} B_{q_2} \int_{-\frac{L_b}{2}}^{\frac{L_b}{2}} f_{p_1}(x) f_{p_2}(x) dx \right] \bullet \bullet \bullet \qquad (3.7)$$

Cross products of the trial functions and their first and second order derivatives have to be integrated between $-\frac{L_b}{2}$ and $\frac{L_b}{2}$. These integrals have been analitically solved for the Psin functions and can be found in appendix D.

$$f_n(x) = \mathrm{Psin}_n\left(\frac{2x}{L_b}\right) \qquad (3.8)$$

These integrals are similar to the one presented by formula (3.9). They can be uselful for other applications and are intended for the reader desirous to use the Psin functions in their applications.

$$\frac{1}{4} F6_{mn}(x) = \int_{x-\frac{L}{2}}^{x+\frac{L}{2}} Psin_m\left(\frac{2x}{L_b}\right) \frac{\partial\, Psin_n\left(\frac{2x}{L_b}\right)}{\partial x} dx \qquad (3.9)$$

The total energy of the system is therefore expressed in term of the *F1*, *F2*, *F3*, *F4*, *F5* and *F6* functions which can be found in appendix D.

$$E = -\omega^2 \frac{\rho_b}{2} h_b \frac{L_b}{8} \sum_{p_1=1}^{P} \sum_{p_2=1}^{P} \left[A_{p_1} A_{p_2} F4_{p_1 p_2}(0, L_b) \right]$$
$$- \omega^2 \frac{\rho_b}{2} \frac{h_b^3}{12} \frac{1}{2L_b} \sum_{q_1=1}^{Q} \sum_{q_2=1}^{Q} \left[B_{q_1} B_{q_2} F1_{q_1 q_2}(0, L_b) \right]$$
$$- \omega^2 \frac{\rho_b}{2} h_b \frac{L_b}{8} \sum_{q_1=1}^{Q} \sum_{q_2=1}^{Q} \left[B_{q_1} B_{q_2} F4_{q_1 q_2}(0, L_b) \right] \bullet \bullet \bullet \qquad (3.10)$$

Performing the variation of E_k and E_p in respect to the coeficients A_n and B_n lead to a set of P+Q linear equations in term of A_n and B_n. These linear equation can be expressed in matrix form as it is presented in equation (3.11).

$$\left[-\omega^2 \begin{pmatrix} M_b^1 & M_b^2 \\ M_b^{2t} & M_b^3 \end{pmatrix} + \begin{pmatrix} K_b^1 & K_b^2 \\ K_b^{2t} & K_b^3 \end{pmatrix} \right] \begin{Bmatrix} A \\ B \end{Bmatrix} = \begin{Bmatrix} 0 \\ 0 \end{Bmatrix} \qquad (3.11)$$

- $M^1$is a PxP matrix, M^2 is a PxQ matrix, and $M^3$is a QxQ matrix
- K^1 is a PxP matrix, K^2 is a PxQ matrix, and $K^3$is a QxQ matrix
- A is the solution vector for the axial displacement (rank P)
- B is the solution vector for the transversal displacement (rank Q)

Each matrix component can be found in appendix E. where the models are printed in details. The equation (3.11) has no solution since there is no excitation in the model. By solving the eigen-value problem, the mode shapes of the beam and the resonant frequencies are obtained.

3.1.2 Experimental and theoretical validation

The accuracy of the simulation tool developed in the previous subsection was validated using an experimental beam, the computation of the exact solution (solving equation (2.1)), and a variational method using polynomials [13].

Table 3.I: Beam used for the validation

Beam	Simply Supported
Length	610 mm
Width	51 mm
Thickness	6.35 mm
Material	Steel
Young Modulus	210 MPa
Density	7800 Kg/m3

The beam characteristics are presented in Table 3.I. A picture of the beam is presented in Figure 3.3. Reflective tape is positioned at twenty three points along the beam in order to take vibration data with a laser vibroneter. Below the ninth point, a symetric piezoelectric actuator is glued on the beam. This piezoelectric patch was excited with white noise [0 to 1600Hz bandwidth] at a voltage of $60V_{rms}$.

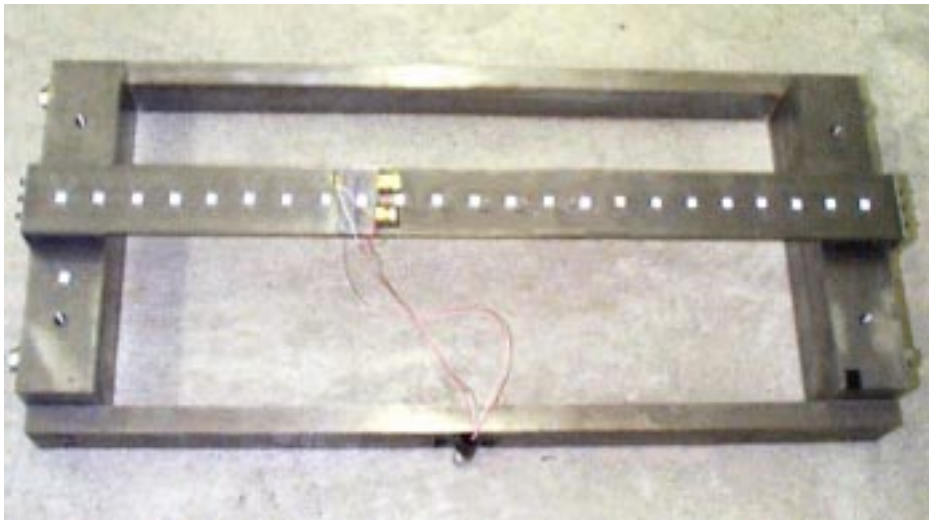

Figure 3.3: Simply supported experimental beam with piezoelectric actuator

The resonance frequencies of the beam are extracted from the vibration data. The mean square velocity of the beam has been computed. The experimental resonance frequencies presented in table 3.II are the local maximums of the mean square velocity. The experimental data is taken as reference to compute the errors for the simulation models. The error is the standard variation of resonance frequency in respect to the measurement $Error = 100*(f_{theory}-f_{experimental})/f_{experimental}$. The error is presented as a percentage of the experimental value. Three theoretical models are compared in table 3.II. The first theoretical model uses the exact solution derived from equation (2.1) and is expressed in equation (3.12)

$$f_n = n^2 \frac{\pi}{2} \sqrt{\frac{c_{11}^b h_b^{\ 2}}{12 \rho_b L_b^4}} \tag{3.12}$$

The second theoretical model is a variational model using polynomials as trial functions. The third one is the model to be validated, using the Psin functions as trial functions. The values for the errors increase with the mode number, showing that the simply supported assumption is not perfectly accurate. However, the accuracy of the three theoretical methods is similar. The performance of a variational method using Psin functions (model III) is similar to the one using polynomials (model II).

Table 3.II: Resonance frequencies of a SS beam

Mode	Experiment (Hz)	Theory I	Error I	Theory II	Error II	Theory III	Error III
1	39.90	40.28	0.95	40.15	0.63	40.15	0.63
2	161.20	161.12	-0.05	160.58	-0.38	160.58	-0.38
3	358.00	362.52	1.26	361.21	0.90	361.22	0.90
4	633.00	644.48	1.81	641.93	1.41	641.98	1.42
5	985.00	1007.00	2.23	1002.58	1.78	1002.74	1.80
6	1413.00	1450.00	2.62	1442.95	2.12	1443.25	2.14

Both models used 20 trial functions, which permit to obtain reasonable solutions for the 10 first modes. Higher modes could be taken into account by increasing the number of trial functions. This is only possible with the new model (III) since the former model (II)

cannot handle more trial functions. Model III accuracy is not limited by numerical errors. Up to 300 trial functions have been used with success. With the two variational methods, the boundary conditions can be adjusted so that the resonant frequencies agree. In this case, the stiffness K_3 and K_6 have been lowered from 5e+9 N/m to 5e+7 N/m.

Table 3.III: Comparison with adjusted model

Mode	Experiment (Hz)	Theory III	Error (%)
1	39.88	40.13	0.63
2	161.2	160.31	-0.55
3	358	359.93	0.54
4	633	637.98	0.79
5	985	993.2	0.83
6	1413	1422.97	0.71

The theory agrees perfectly with the experiment since the error is always smaller than one percent. This demonstrates the adaptability of the variational method.

3.2 Piezoelectric layer

The model used for the piezoelectric layer is derived from the work of *F. Charette et al.* [13]. The same displacement field was used. The model was derived using the Psin functions as trial functions.

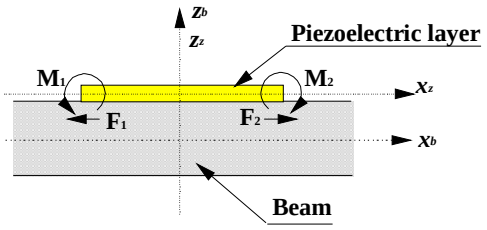

Figure 3.4: Diagram of a piezoelectric layer on a beam

Figure 3.3 presents the configuration in which the piezoelectric layer is modeled. This asymetric configuration induces motion of the beam in the axial and transversal direction.

In a simplier model, the piezoelectric layer can be modeled as two moments M_1, M_2, and two axial forces F_1,F_2. The global displacement of a point of the piezoelectric layer is described in equation (3.13).

$$\begin{cases} U_z(x,z_z,\tau) = u_b(x,\tau) - \left(z_z + \frac{1}{2}(h_b + h_z)\right)\frac{\partial w_b(x,\tau)}{\partial x} \\ W_z(x,z_z,\tau) = w_b(x,\tau) \end{cases} \tag{3.13}$$

The displacements were derived using continuity between the beam and the piezoelectric layer. It is assumed that no sliding occurs at the interface between the beam and the piezoelectric layer. This assumption allows the change of variable z_b=z_z+1/2(h_b+h_z). With this change of variable, the equation (3.13) is very easily derived from equation (3.1). The expression for the enthalpy density [45] differs from the beam model. This changes the expression for the potential energy as it can be seen in equation (3.14). In this expression, the Einstein notation for summations is used.

$$E_p^z = \int_V \left[\frac{1}{2} c_{ij}^z S_i^z S_j^z - e_{kl}^z G_k^z S_l^z - \frac{1}{2} \in_{mn}^z G_m^z G_n^z\right] dv \tag{3.14}$$

Two other terms are added to the mechanical enthalpy. Only the second term changes the model noticeably. The third term is a constant in space and is lost when the variation is performed. The derivation of this model is not much different than for the beam alone except that more terms are involved. The matrices $[M_z]$, $[K_z]$ and the force vector $\{F_z\}$ corresponding to the piezoelectric layer can be found in appendix. No major differences were noticed compared to the previous model of *F. Charette et al.* [13].

3.3 Constrained layer damping

3.3.1 Theory

A model for the constrained layer damping has been developed since the general design is quite similar to a distributed absorber. The simulation approach is different since the physical phenomenon taken into account is also different. The main goal in having a constrained layer damping on top of a structure is to increase the damping of the all base structure. The core of the constrained layer damping is made of visco-elastic material that will be stressed mainly with shear. The visco-elastic layer dissipates energy by heating. Since the model of the beam did not take into account the shear, a new function $\phi_c(x)$ has to be introduced for the visco-elastic layer.

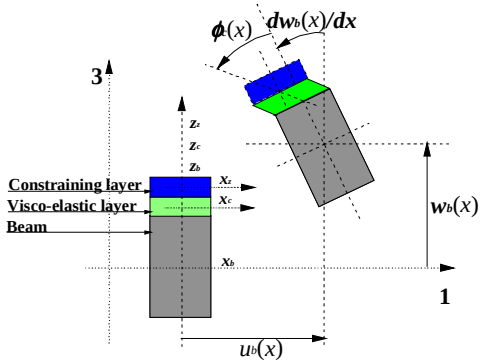

Figure 3.5: Displacement field for a constrained layer

According to Midlin theory, ϕ_c is the shear angle in the considered layer. This is a hybrid model since the beam and the piezoelectric layer are modeled according to Bernoulli-Euler theory (no shear assumption).

$$\phi_c(x) = \sum_{r=1}^{R} C_r \, Psin_r\left(\frac{2x}{L_b}\right) \tag{3.15}$$

The constraining layer can have piezoelectric properties as suggested by *A. Baz and J. Ro* [47]. For this reason, this layer will be indexed with the letter z.

$$\begin{cases} U_c(x,z_c,\tau) = u_b(x,\tau) - \left(z_c + \frac{1}{2}(h_b + h_c)\right)\frac{\partial w_b(x,\tau)}{\partial x} - \left(z_c + \frac{h_c}{2}\right)\phi_c(x,\tau) \\ W_c(x,z_c,\tau) = w_b(x,\tau) \end{cases} \tag{3.16}$$

Equation (3.16) presents the global displacement of a point of the visco-elastic layer. It is very similar to equation (3.13) except for the last term of U_c. This last term introduces the shear influence in the displacement of the point.

$$\begin{cases} U_z(x,z_z,\tau) = u_b(x,\tau) - \left(z_z + \frac{1}{2}(h_b + 2h_c + h_z)\right)\frac{\partial w_b(x,\tau)}{\partial x} - h_c\phi_c(x,\tau) \\ W_z(x,z_z,\tau) = w_b(x,\tau) \end{cases} \tag{3.17}$$

Equation (3.17) describes the global displacement of a point of the constraining layer. The shear in the visco-elastic layer also introduces a third term for U_z.

$$\begin{cases} S_1^c(x,z_c,\tau) = \frac{\partial u_b(x,\tau)}{\partial x} - \left[z_c + \frac{1}{2}(h_b + h_c)\right]\frac{\partial^2 w_b(x,\tau)}{\partial x^2} - \left(z_c + \frac{h_c}{2}\right)\frac{\partial \phi_c(x,\tau)}{\partial x} \\ S_5^c(x,z_c,\tau) = \phi_c(x,\tau) \\ S_2^c = S_3^c = S_4^c = S_6^c = 0 \end{cases} \tag{3.18}$$

Equation (3.18) presents the strains of the visco-elastic layer. In this model two strains are taken into account, S_1 and S_5. It is interesting to notice that the choice of ϕ_c as a new unknown function simplifies the expression of S_5.

$$\begin{cases} S_1^z(x,z_z,\tau) = \dfrac{\partial u_b(x,\tau)}{\partial x} - \left[z_z + \dfrac{1}{2}(h_b + 2h_c + h_z) \right] \dfrac{\partial^2 w_b(x,\tau)}{\partial x^2} - h_c \dfrac{\partial \phi_c(x,\tau)}{\partial x} \\ S_2^z = S_3^z = S_4^z = S_5^z = S_6^z = 0 \end{cases} \tag{3.19}$$

Equation (3.19) presents the strain of the constraining layer. It is not very different from the expression derived for the beam (3.2). Only shear is added to S_1. From equations (3.16) to (3.19) the global matrix equation (3.20) is derived.

$$\left[-\omega^2 \begin{pmatrix} M^1 & M^2 & M^4 \\ M^{2t} & M^3 & M^5 \\ M^{4t} & M^{5t} & M^6 \end{pmatrix} + \begin{pmatrix} K^1 & K^2 & K^4 \\ K^{2t} & K^3 & K^5 \\ K^{4t} & K^{5t} & K^6 \end{pmatrix} \right] \begin{Bmatrix} A \\ B \\ C \end{Bmatrix} = \begin{Bmatrix} F^1 \\ F^3 \\ F^6 \end{Bmatrix} \tag{3.20}$$

The coefficients of vector C are related to ϕ_c (cf. equation (3.15)). The motion of the all system is known once the vector *A*, *B* and *C* are solved for.

3.3.2 Simulation example

This simulation refers to *A. Baz and J. Ro* work. They use a finite element approach to model a beam with an active constrained layer damping treatment (ACLD).

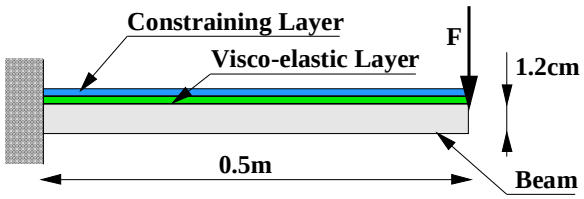

Figure 3.6: Clamped-free beam with full ACLD treatment

Figure (3.6) presents the simulation beam with its ACLD treatment. The details of the properties used to model this system are presented in Table 3.IV. Most of these properties are extracted from the article [48]. The numerical indicator used to show the performance

of the constrained layer is the compliance (motion of the tip of the beam with an excitation at the same point).

Table 3.IV: Properties of modeled system

	Clamped Free Beam	**Visco-elastic Layer**	**Constraining Layer**
Length	500 mm	500 mm	500 mm
Width	50 mm	50 mm	50 mm
Thickness	12.5 mm	27.5 mm	2.5 mm
Material	Steel	visco-elastic material	PZT
Young Modulus C_{11}	210 MPa	1e+7+i1e+5 Pa	63 MPa
C_{55}		1.1e+8+i1.1e+8 MPa	
Density	7800 Kg/m^3	1000 Kg/m^3	7600 Kg/m^3

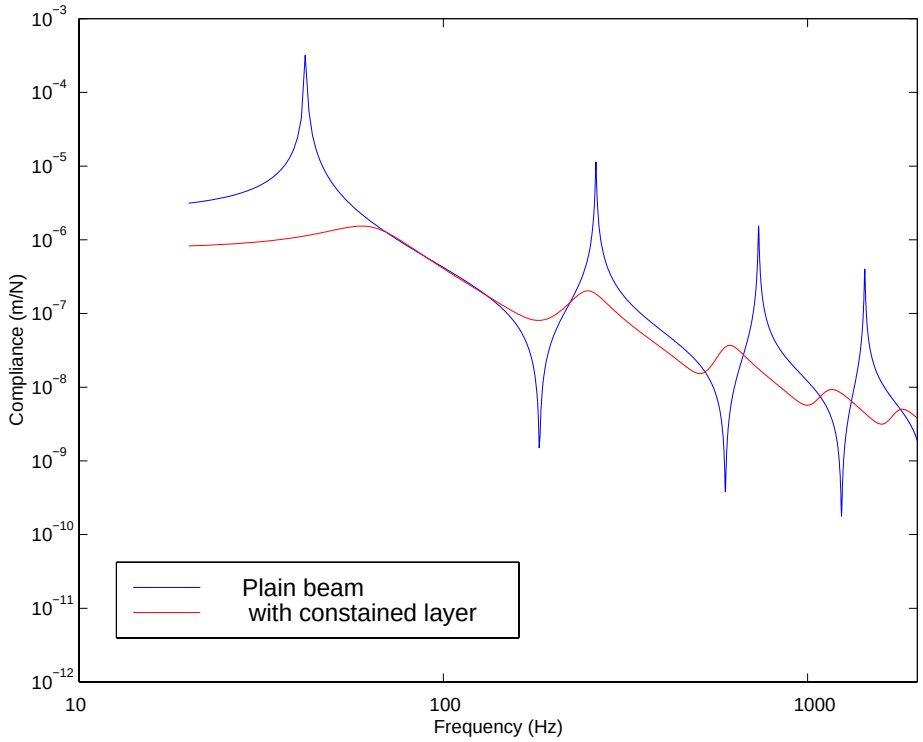

Figure 3.7: Damping of a beam using a constrained layer

Figure (3.7) presents the compliance in respect to frequency calculated using the method of this thesis. In this special case, the frequency scale is logarithmic. The performance of the constrained layer damping is impressive at reducing the peaks of resonance. This

performance is expected since the visco-elastic material has more than twice the thickness of the beam itself. The weight added by the constrained layer damping represents 50% of the beam alone. This can be seen by the drift of the resonance frequencies.

Baz and Ro used a different method of analysis for the same problem and their results are given in Appendix B. The agreement between Figures 3.7 and B.1 is not perfect since many parameters of Baz and Ro's work were not specified. However the comparison of the two methods lends support to the validity of the model of this thesis.

3.4 Absorbers

3.4.1 The point absorber

A point absorber is defined as mass-spring system, which is connected at one point on the beam. An absorber with a connection to the beam which has a small length compared to the wavelength of the beam response can be considered as a point absorber. The model presented below is for passive absorbers. For this model the motion of the absorber mass w_m differs from the transversal displacement of the beam w_b.

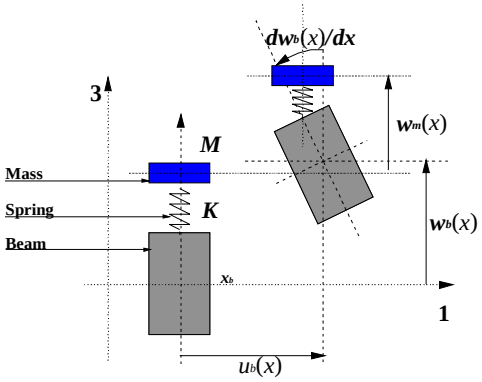

Figure 3.8: Displacement field of a beam with a point absorber

Figure 3.8 presents the displacement field of the slice of beam supporting the absorber. As a first approximation, the rotation of the absorber mass is not taken into account in this model. The stiffness of the spring K is complex in order to model damping. The displacement field of the beam is unchanged compared to Figure 3.2. The absorber is considered as added impedance on the beam. w_m can then be determined from equation (3.21) without introducing a new variable in the system .

$$K(w_m - w_b) = Z(-j\omega w_b) \tag{3.21}$$

Simplifying equation (3.21), a simple proportionality relationship between w_m-w_b and w_b is obtained and is presented in equation (3.22).

$$w_m - w_b = Dw_b \tag{3.22}$$

$$with \quad D = \frac{\alpha^2}{1-\alpha^2}, \quad \alpha = \frac{\omega}{\omega_r} \quad and \quad \omega_r = \sqrt{\frac{K}{M}}$$

The variable *D*, which is introduced in this equation, is frequency dependent. The virtual work of a point absorber is then easily computed. It is the restoring force of the spring multiplied by the transversal motion of the beam. The virtual work of the absorber is expressed in equation (3.23)

$$Fw_b = KDw_b^2 \delta(x - x_a) = KD \sum_p \sum_q B_p B_q P\,sin_p\left(\frac{2x_a}{L_b}\right) P\,sin_q\left(\frac{2x_a}{L_b}\right) \tag{3.23}$$

The variation of the virtual work (in respect to B_n) gives the elements of the matrix describing the absorber energy.

$$K^a_{p,q} = KD\,P\,sin_p\left(\frac{2x_a}{L_b}\right) P\,sin_q\left(\frac{2x_a}{L_b}\right) \tag{3.24}$$

These matrix elements are added in equation (3.11) in order to solve for the coupled system beam + absorber.

3.4.2 *The "small" distributed absorber*

Figure 3.9 presents the displacement field of a beam with a small absorber on top of it. The elastic layer of the absorber is constrained in the 1 and 3 direction. The mass of the absorber is moving as a block and the transversal motion of the center of the mass is $w_m(x)$.

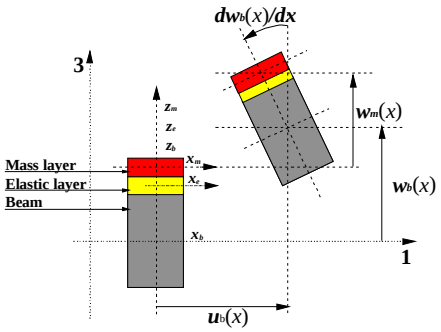

Figure 3.9: Displacement field of a small absorber on a beam

This slightly more complex model assumes that the mass extends on a small portion of the beam in comparison to the wavelength of the excitation. In this model, the Poisson ratio is taken into account. From equation (3.22) and using conditions of continuity at each interfaces the displacement field and stress field can be derived for the elastic and the mass layer:

$$\begin{cases} U_e(x,z_e,\tau) = u_b(x,\tau) - \left(z_e + \frac{1}{2}(h_b + h_e)\right)\frac{\partial w_b(x,\tau)}{\partial x} \\ W_e(x,z_e,\tau) = \left[1 + \frac{1}{h_e}\left(z_e + \frac{h_e}{2}\right)D\right] w_b(x,\tau) \end{cases} \tag{3.25}$$

Equation (3.25) presents the global displacement of a point of the elastic layer. The axial motion is similar to a piezoelectric layer (cf. equation (3.13)). The transversal motion is a linear interpolation between the motion of the beam and the motion of the absorber mass.

$$\begin{cases} U_m(x,z_m,\tau) = u_b(x,\tau) - \left(z_m + \frac{1}{2}(h_b + 2h_e + h_m)\right)\frac{\partial w_b(x,\tau)}{\partial x} \\ W_m(x,z_m,\tau) = [1+D]w_b(x,\tau) + \nu\left[u_b(x,\tau) - \left(z_m + \frac{1}{2}(h_b + 2h_e + h_m)\right)\frac{\partial w_b(x,\tau)}{\partial x}\right] \end{cases} \tag{3.26}$$

Equation (3.26) presents the global displacement of a point of the absorber mass. The contribution of the Poison ratio is added to the transversal motion. The Poisson ratio was considered critical for this term only. The reason is that the kinetic energy of the system is primarily affected by the transversal motion of the absorber mass.

$$\begin{cases} S_1^e(x,z_e,\tau) = \dfrac{\partial u_b(x,\tau)}{\partial x} - \left[z_e + \dfrac{1}{2}(h_b + h_e) \right] \dfrac{\partial^2 w_b(x,\tau)}{\partial x^2} \\ S_3^e(x,z_e,\tau) = \dfrac{1}{h_e} D w_b(x,\tau) + \nu \left[\dfrac{\partial u_b(x,\tau)}{\partial x} - z_e + \dfrac{1}{2}(h_b + h_e) \dfrac{\partial^2 w_b(x,\tau)}{\partial x^2} \right] \\ S_2^e = S_4^e = S_5^e = S_6^e = 0 \end{cases} \quad (3.27)$$

The equation (3.27) presents the strain of the elastic layer. The Poisson ratio appears only in S_3 for simplification purposes. The potential energy of the system is being affected primarily by the transversal compression of the elastic layer. The elastic layer is constrained in two directions. The only coupling modeled is the effect of S_1 on S_3 due to the Poisson ratio effect. No shear is assumed in the elastic layer therefore $S_5^e = 0$. An improved model of the absorber could include the theory developed for the constrained layer damping. The model also neglects the stresses in the mass, therefore, the strains for the mass layer are of no interest. The mass material is assumed to have a small modulus of elasticity and the mass layer a small thickness compared to the beam. For these reasons, the potential energy of the mass layer is neglected in respect to the potential energy of the beam. From the equations (3.25) to (3.27) the final matrix system can be derived:

$$\left[-\omega^2 \left(\left[M_{cnst}^a \right] + D\left[M_D^a \right] + D^2 \left[M_{D2}^a \right] \right) + \left(\left[K_{cnst}^a \right] + D\left[K_D^a \right] + D^2 \left[K_{D2}^a \right] \right) \right] \begin{Bmatrix} A \\ B \end{Bmatrix} = \left\{ F_{cnst}^a \right\} \quad (3.28)$$

This equation of motion is significantly different from equations (3.11) or (3.21) because of the D factor which induces a varying mass and stiffness matrix in respect to ω By

solving this matrix equation, the vectors *A* and *B* can be found. The motion of the beam is then entirely known.

3.4.2 Distributed active vibration absorber with constant mass distribution

A model for the "small" absorber is not yet the model expected for a distributed absorber as it was discussed in chapter 2 (figure 2.11). As can be seen Figure 3.10, the mass is constant along the absorber. This model is very important for modeling the distributed absorber with varying mass distribution. For this model, the displacement field remains the same as Figure 3.6. The model has been simplified since the Poisson ratio is no longer taken into account.

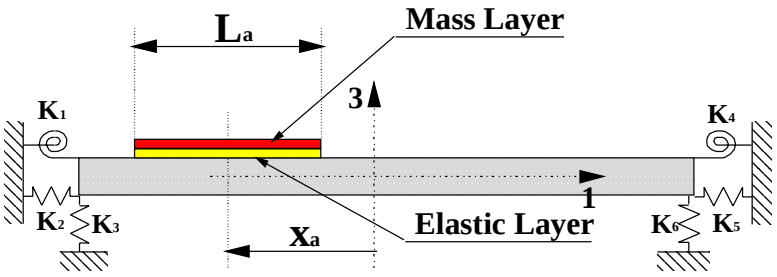

Figure 3.10: Distributed active vibration absorber with constant mass distribution

Figure 3.10 presents the configuration of the distributed active vibration absorber (DAVA) on top of the modeled beam. In this model the length L_a of the absorber is not limited. The abscise of its center point is called x_a. The equations for this model use the transversal displacement of the mass layer w_m as a new unknown function. Therefore, this derivation has many similarities with the one done for the constrained layer in Chapters 3 and 4.

$$w_m(x) = \sum_{r=1}^{R} C_r \, Psin_r\left(\frac{2x}{L_b}\right) \tag{3.29}$$

As for u_b and w_b, w_m is described using the Psin functions. Equation (3.29) presents the approximation of w_m with the R first Psin functions. The rank of the problem is now $P+Q+R$.

$$\begin{cases} U_e(x,z_e,\tau) = u_b(x,\tau) - \left(z_e + \frac{1}{2}(h_b + h_e)\right)\frac{\partial w_b(x,\tau)}{\partial x} \\ W_e(x,z_e,\tau) = w_b(x,\tau) + \frac{1}{h_e}\left(z_e + \frac{h_e}{2}\right)(w_m(x,\tau) - w_b(x,\tau)) \end{cases} \tag{3.30}$$

Equation (3.30) presents the global displacement of a point of the elastic layer. The axial displacement is unchanged compared to equation (3.27). The transversal displacement is a linear interpolation between the motion of the beam w_b and the motion of the mass layer w_m.

$$\begin{cases} U_m(x,z_m,\tau) = u_b(x,\tau) - \left(z_m + \frac{1}{2}(h_b + 2h_e + h_m)\right)\frac{\partial w_b(x,\tau)}{\partial x} \\ W_m(x,z_m,\tau) = w_m(x,\tau) \end{cases} \tag{3.31}$$

Equation (3.31) presents the global displacement of a point of the mass layer. The expression of the axial displacement is similar to equation (3.26). The introduction of the new variable w_m simplifies completely the expression of the transversal displacement W_m.

$$\begin{cases} S_1^e(x,z_e,\tau) = \frac{\partial u_b(x,\tau)}{\partial x} - \left[z_e + \frac{1}{2}(h_b + h_e)\right]\frac{\partial^2 w_b(x,\tau)}{\partial x^2} \\ S_3^e(x,z_e,\tau) = \frac{1}{h_e}(w_m(x,\tau) - w_b(x,\tau)) \\ S_2^e = S_4^e = S_5^e = S_6^e = 0 \end{cases} \tag{3.32}$$

Equation (3.32) presents the strains of the elastic layer. The axial strain S_1 is similar to equation (3.27). The strain in the transversal direction is constant. No coupling between

the two axis of load is modeled. In order to introduce the active part in the model, the elastic part is treated as a piezoelectric layer. Its potential energy is computed using equations (3.14) and (3.32). The final equation to be solved is similar to equation (3.20). Each element of the matrices of equation (3.20) can be found in appendix E.

3.4.3 Theoretical Validation

An exact solution for a beam with a point absorber does exist. This is done using equation (2.1) and a modal expansion. This derivation process is described in detail in appendix C. Four different methods were compared on a test case;

- Exact solution truncated to N first modes
- Variational method for a point absorber
- Variational method for a small absorber (taking into account the Poisson ratio)
- Variational method for a distributed absorber with constant mass distribution

The configuration for this test is a single absorber positioned in the middle of a simply supported beam. The properties of the beam used for the simulation are presented table 2.I. The excitation is a piezoelectric patch positioned as presented in Figure 3.11.

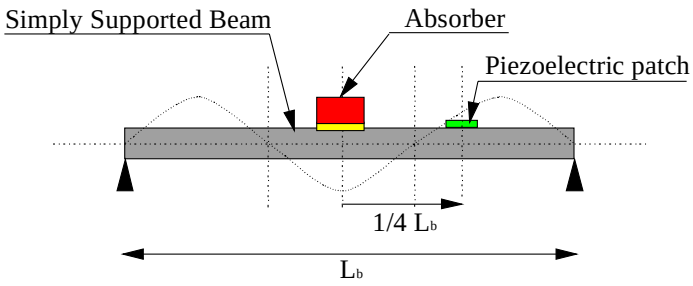

Figure 3.11: Configuration for absorber model validation

Figure 3.11 presents the configuration for which the models will be tested. The absorber does not change, only its model does. For this reason, it is called a point absorber, a small absorber or a large absorber depending on the model.

Table 3.V: Absorber for model comparison

Mass	2.7 g
Length	3 mm
Width	25 mm
MassThickness	3 mm
Mass density	11300 kg/m^3
Spring Thickness	1 mm
Spring Density	1470 kg/m^3
Spring Stiffness	9E+5 + i 9E+3
Poisson Ratio	0.28
Resonance	820 Hz

The details of the absorber properties are presented in Table 3.V. The absorber has a width small enough to be considered as a point absorber. The radiated power of the beam was computed over the frequency range [0 to 1600Hz]. Using the equations of Appendix Figure 3.11 presents the acoustic response of the beam alone and with the absorber. The absorber action is typical. The third mode for which the absorber is almost tuned into two different degrees of freedom with higher and lower resonant frequencies. The absorber significantly modifies the dynamics of the beam over a small frequency range. For this reason the comparison is made between 600 and 1000 Hz and is presented Figure 3.12. The differences between the four models are very small. A slight change of the peak value of the second third mode is noticeable. Introducing the Poisson ratio adds very little changes around the resonance frequency of the absorber. The absorber for this comparison has the ideal width to thickness ratio for the Poisson effect to appear. When the absorber will be larger, this effect becomes negligible. For this reason, the Poisson ratio was neglected in later models. This comparison validates partially the four models. To validate properly these models, experiments have been conducted. This experimental validation is presented in chapter 4. along with the prototypes.

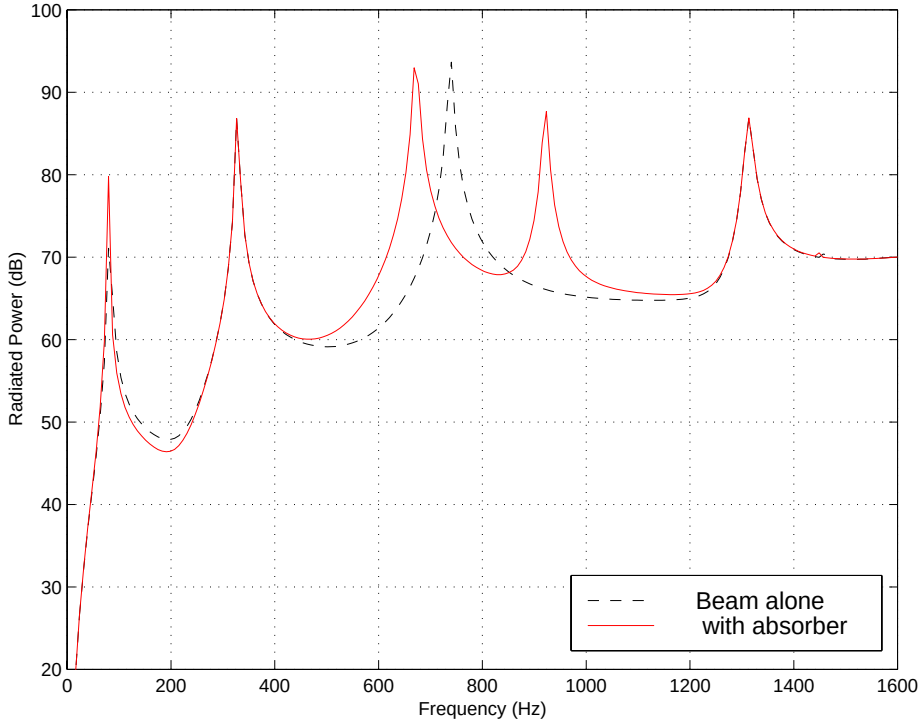

Figure 3.12: Acoustic response of beam with an absorber.

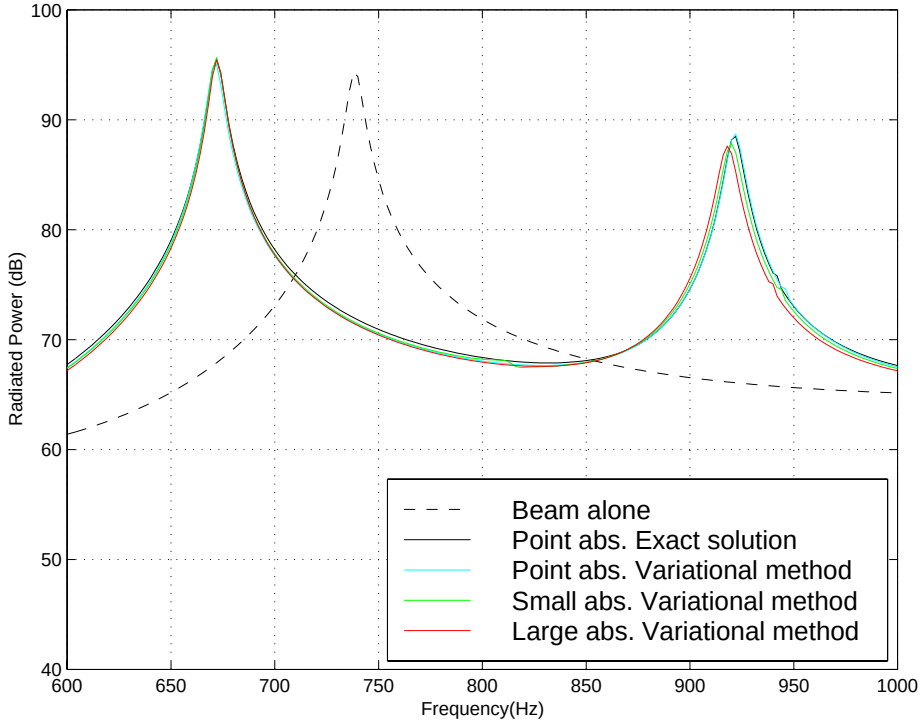

Figure 3.13: Comparison between four different models

3.5 Distributed absorber

The main goal for the previous developments was to obtain a model for an active-passive distributed absorber. The equation manipulations that the former models involved could have been discouraging. However, the time needed to derive, program and troubleshoot the different equations was still reasonable since all the developments involved the same sub-functions *F1, F2*…(cf. Appendix D). Deriving the fully distributed model was at first considered unfeasible since it would involve integrals of the third order (see equation (3.33)).

$$\frac{1}{8L_b} E1_{pqr}(x) = \int_{x-\frac{L}{2}}^{x+\frac{L}{2}} Psin_p\left(\frac{2x}{L_b}\right) \frac{\partial\, Psin_q\left(\frac{2x}{L_b}\right)}{\partial x} \frac{\partial\, Psin_r\left(\frac{2x}{L_b}\right)}{\partial x} dx \qquad (3.33)$$

The idea was to use the large absorber model to obtain a discretized version of distributed absorber. This model is satisfying on a mathematical point of view but it does seem a little far from the physics. The model of the absorber with a varying mass distribution was therefore derived and presented in Section 3.5.2.

3.5.1 Discretized model

This model is based on the distributed absorber presented in *3.4.2*. These absorbers can be positioned all along the beam and have their mass differ from each other. Increasing the number of these absorbers on the beam in the limit will create a distributed absorber as is pictured in Figure 3.14. The behavior of the infinitely small absorbers is in this case is independent from each other but is dependent upon the continuous beam upon which they are positioned. The mass layer does not have any stress in the transversal direction. In this case the mass layer behaves like a fluid (a powder also has this type of property). The original concept for the distributed vibration absorber is that the elastic layer and the mass layer would be in one piece. The model of 3.4.2 thus is not yet appropriate to model

a distributed absorber with a varying mass distribution. To capture the physics the vibration of each mass has to be linked with its adjacent neighbors.

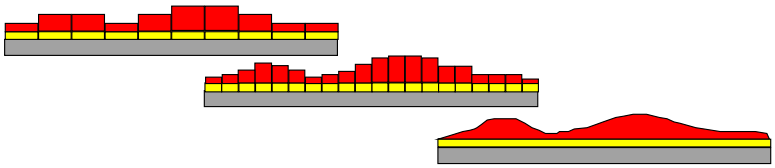

Figure 3.14: Toward a distributed absorber

Considering the boundary conditions between each independent absorber could be a solution but this needs as many w_m functions as there is absorbers. No convergence is ever obtainable since the matrices will grow bigger with the number of absorbers. The only thing known is that the solution is continuous. The idea for solving this problem is to use the Psin functions as a basis to describe the motion of the absorber. This is legitimate since the Psin functions are able to describe any continuous function on the length of the beam. One possible approach would be to truncate the set of Psin functions as it was done for w_b. Since the motion of the beam was described with a truncated set and taking the assumption that the mass distribution is described with the same set, it seemed reasonable to assume the solution to be sufficiently accurate with the same truncated set. The solution using the only assumption of continuity exists and is unique. It is therefore the solution that was looked for. The only true objection is that none of the stresses in the mass layer is taken into acccount. These stresses were considered as neglible from the start of the investigation. This is due to special considerations on the absorber itself. Let us assume that an absorber has a weigth of 10% of a main structure. If it is a distributed absorber this ratio is also true per unit area. If the material used for the mass is the same as the one of the main structure, the thickness of the mass layer is 10% the one of the main structure. If the chosen material is heavier, this would lead to a mass layer even thinner. The beam is modeled according to the Bernoulli-Euler theory also called the “thin beam” theory. A layer which thickness is neglible compared to the thickness of the beam could be modeled as a string. As it will be presented in chapter 4, the constructed prototype placed on a steel beam has a mass layer made of thin sheets of

lead. It agrees perfectly with this theory where stresses are neglected within the mass layer. As a last justification to this approach, comparison with experiments and with the model presented in *3.5.2* validated the model.

Almost no modification is therefore needed to the model presented in 3.4.2. w_m is a unique function that describes the motion of all the masses at once. The mass and stiffness matrices of each discrete absorber are just added one to the other. The only noticeable change is the number of coeficients describing w_m. For a small absorber typically 1 to 3 coeficients were needed. With more coeficients the system becomes over-determined, the matrices are singular and cannot be inverted. For a large distribution, 30 to 60 coeficients were used.

3.5.2 Distributed model

The mass distribution is coded using the Psin functions. h_m is the thickness of the mass layer. Given below,

$$h_m(x) = \sum_{s=1}^{S} d_s \, Psin_s\left(\frac{2x}{L_b}\right) \tag{3.34}$$

This time, the coefficients d_s are known. The only part in which this formulation affects the model presented in *3.4.3* is the kinetic energy of the mass layer.

$$E_k^m = \tfrac{1}{2} b \rho_m \int_{x_a - \frac{L_a}{2}}^{x_a + \frac{L_a}{2}} \int_{-\frac{h_m(x)}{2}}^{\frac{h_m(x)}{2}} \left\{ \left[u_b(x) - \left[z_m + \tfrac{1}{2}\left(h_b + 2h_e + h_m(x)\right) \right] \frac{\partial w_m(x)}{\partial x} \right]^2 + \left[w_m(x) \right]^2 \right\} dz_m dx \tag{3.35}$$

For the integral with respect to x, $(h_b+2h_e+h_m(x))$ is approximated to $(h_b+2h_e+h_m)$ with h_m being the average value of $h_m(x)$ (first order approximation). The equation (3.35) is linearized and presented in equation (3.36).

$$E_k^m = \tfrac{1}{2} b \rho_m \int_{x_c - \frac{L_a}{2}}^{x_a + \frac{L_a}{2}} \left\{ h_m(x) u_b^2(x) - (h_b + 2h_e + h_m) h_m(x) u_b(x) \frac{\partial w_b(x)}{\partial x} \right.$$

$$\left. + \left[\frac{h_m^2}{12} + \frac{1}{4}(h_b + 2h_e + h_m)^2 \right] h_m(x) \left(\frac{\partial w_b(x)}{\partial x} \right)^2 + h_m(x) w_m^2(x) \right\} dx \qquad (3.36)$$

Three functions of third order have to be integrated. One of these integrals is presented in equation (3.33). The kinetic energy can then be described in term of a linear combination of A_p, B_q and C_r (cf. equation (3.10)). After obtaining the Lagrangian and performing the variation in respect to A_p, B_q and C_r, the global matrix equation similar to equation (3.20) is obtained.

3.5.3 Model comparison

The two models were tested with the beam presented in Table 3.I. The distribution of the mass is similar to the 7th Psin function (cf. figure 2.12). The stiffness of the elastic layer is 7.5e+5+i4.5e+5 N/m for a thickness of 2 mm. The overall mass of the absorber represent 10% of the beam mass.

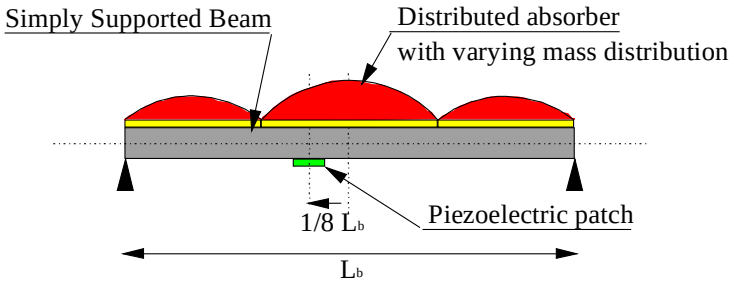

Figure 3.15: Distributed absorber with varying mass distribution

Figure 3.15 presents the configuration of the beam and the DAVA with varying mass distribution. The excitation is provided by a piezoelectric patch positioned on the underside of the beam. Figure 3.15 presents the mean square velocity (defined as the sum

of the modules squared of the normal velocity divided by the number of measurement points) of the beam from 0 to 1600Hz. The six first modes of the beam alone (bare beam) can be seen with the response shown by the dash line. The natural resonance frequency of the DAVA is very high. For this reason only the fifth and sixth mode of the beam are affected by the DAVA.

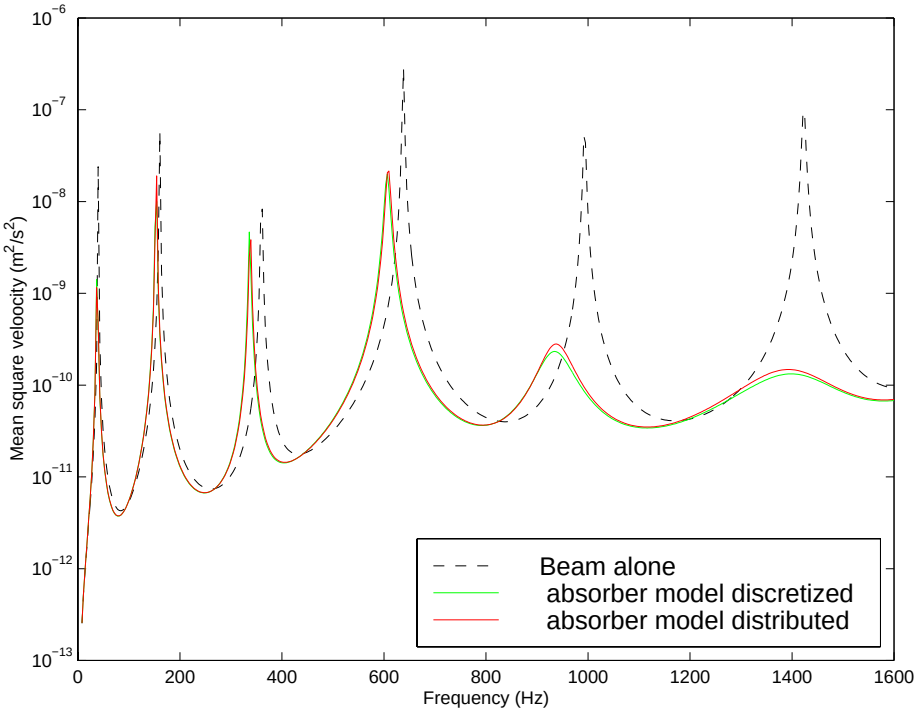

Figure 3.16: Comparison between two models of distributed absorber

The two models are seen from Figure 3.16 to match almost perfectly. The asumptions done for both models are slightly diferent so the small changes for the peak values at 950Hz and 1400Hz are understandable. The experimental validation for these models is presented in chapter 4.